Co-published by
Institute of Fluid-Flow Machinery
Polish Academy of Sciences
Committee on Thermodynamics and Combustion
Polish Academy of Sciences

http://www.imp.gda.pl/archives-of-thermodynamics/

Linear method for the determination of Newton's heat transfer coefficient in the gap under conditions of limited convection

Ewa Pelińska-Olko*, Emilija Zagórska

Department of Thermodynamics and Renewable Energy Sources, Faculty of Mechanical and Power Engineering, Wroclaw University of Science and Technology, Wybrzeże Stanisława Wyspiańskiego 27, 50-370 Wrocław, Poland
*Corresponding author email: Ewa.Olko@pwr.edu.pl

Received: 21.02.2025; revised: 16.05.2025; accepted: 27.05.2025

Abstract

This study investigates heat transfer under conditions of limited (undeveloped) convection within a narrow 5 cm gap between a centrally positioned heater and the inner walls of a closed chamber. A simplified approach − the linear method − is proposed for estimating Newton's heat transfer coefficient, assuming a weak linear dependence on temperature. Experimental data and known convection models were used to verify the method. The convective component obtained using the linear method was compared to experimental values and theoretical bounds, showing that the linear method slightly overestimates but remains within a valid range. Artificial neural networks supported the estimation of steady-state temperatures and voltages. This work is a continuation of earlier research and confirms the practical value of the linear method in constrained thermal environments. Further development of the experimental rig is planned to expand the study.

Keywords: Limited convection; Gap; Artificial neural network; Newton heat transfer coefficient

Vol. 46(2025), No. 2, 153–165; doi: 10.24425/ather.2025.154914

Cite this manuscript as: Pelińska-Olko, E., & Zagórska, E. (2025). Linear method for the determination of Newton's heat transfer coefficient in the gap under conditions of limited convection. *Archives of Thermodynamics*, 46(2), 153−165.

1. Introduction

Convection refers to the macroscopic movement of fluid molecules—liquids and gases—with specific velocity profiles [1]. It is classified as either natural, driven solely by gravitational forces, or forced, involving additional external forces [2]. The phenomenon arises from the imbalance between buoyancy forces, resulting from temperature-dependent density variations, and viscous forces [3]. Instabilities in the fluid lead to the formation of convective cells, first described by Bénard (see Aubin [3]). Rayleigh-Bénard convection occurs when the lower fluid layers are hotter than the upper ones. Such structures, resembling biological cells, are observed in Newtonian and non-Newtonian fluids, in homogeneous liquids and in nanoparticle suspensions [4]. Nanoparticles added to the base fluid may be metallic, such as Al_2O_3 or Cu [5], or non-metallic, such as SiO_2 [6].

Convection processes occur at both large scales, such as in stellar interiors [7], and in small-scale systems with complex geometries. Applications include nuclear reactor design and electronics cooling systems [8]. Experimental methods, such as the Schlieren technique, which is an optical method, allow for imaging the flow of liquids with different densities [9].

The presence of obstacles can influence the convective flow, modifying the structure of the thermal boundary layer and affecting heat transfer rates above or below a horizontally placed plate [10]. In particular, obstacles below a horizontally placed plate can lead to laminarization and thickening of the boundary

Nomenclature

A – area of surface, m^2
B, C, D, E – constants
Gr – Grashof number
h – Newton's coefficient, W/(m^2 K)
m – number of neurons
Nu – Nusselt number
P – power, W
Pr – Prandtl number
$\dot{Q}$ – heat flux, W
R – electrical resistance, Ω
R^2 – coefficient of determination
$r_{y_{ei}y_i}$ – Pearson's coefficient
T – temperature, K
t – time, s
U – voltage, V

Greek symbols

δ – thickness of a gap, m
ε – relative emissivity coefficient
ε_z – correction factor
λ – thermal conductivity, W/(m K)
σ – Stefan-Boltzmann constant, W/(m^2 K^4)

Subscripts and Superscripts

b – solid body
f – fluid
ch – chamber
k – convection part
h – heater
r – radiation part
S – using Solver function
tgc – theoretical gap model
toc – theoretical open model

Abbreviations and Acronyms

ANN – artificial neural networks
GNU R – interpreted language
GPL – general public license
HL – hidden layer
IN – input layer
ML – linear method
OUT – output layer
SEM – electromotive force
RMSE – root mean square error
TB – training base

layer, decreasing the heat transfer coefficient [11]. The concept of the thermal boundary layer was introduced by Prandtl and remains essential for understanding convection phenomena. The Prandtl number (Pr) expresses the ratio of momentum diffusivity to thermal diffusivity, with heat conduction dominating within the thermal boundary layer [12].

Scaling effects of convective cells, involving their expansion or contraction with volume changes, significantly impact thermal resistance in engineering structures. Key factors include gap dimensions, wall displacement and temperature differences, which collectively influence convective patterns [13]. Convection in rotating [14] and stationary [15] partitions has been studied experimentally, with results generalized for practical applications [16]. These findings are especially important for industrial systems and modern construction technologies [17].

Given the widespread occurrence and technological significance of natural convection, continued research in this area remains fully justified. Moreover, the development of methods for analysing thermal phenomena on a small scale − particularly in closed or semi-closed spaces − has increased the need for a deeper understanding of heat transport mechanisms in narrow gaps. This is driven by technological demands, as many modern applications tend toward component miniaturization, such as in microelectronics, materials engineering, and the design of advanced passive cooling systems. In such confined geometries, classical convection models often prove insufficient. This further reinforces the relevance and justification of the research topic undertaken in this study.

In the present study, the term 'convection' refers specifically to natural convection in Newtonian fluids, where viscosity depends only on temperature. This work builds upon previous studies involving the experimental determination of the emissivity of black paint to assess the radiative component of the convection coefficient in this study (h_r) [18], as well as the use of artificial neural networks (ANN) for predicting steady-state temperature distributions within the analysed range of heater power [19].

2. Theory

The basic equation describing the phenomenon of heat transfer between a fluid and a solid body is the energy balance equation for a system with a "lumped capacitance model". This model is used under the assumption that the whole body has a uniform temperature, which changes only in time – and not in space (no temperature gradients in the body). In its general form, this equation represents the change in enthalpy of the body, which affects the change in temperature and enthalpy of the body fluid environment, which can be written in the form of Newton's classical equation. After taking into account the radiation from the body to other material bodies, the energy balance has the form known from the literature Eq. (1) [2]:

$$\begin{cases} mc_p \frac{d\theta}{dt} = hA_h\left(T_h - T_f\right) \\ hA_h\left(T_h - T_f\right) = h_k A_h\left(T_h - T_f\right) + \varepsilon\sigma A_h\left({T_h}^4 - {T_{ch}}^4\right), \end{cases} \quad (1)$$

where: $mc_p \cdot d\theta/dt$ is the enthalpy change of the considered body with mass m and specific heat c_p, and the change in temperature over time measured in its centre $d\theta/dt$; h is the convection coefficient, A_h and T_h are the surface area of the solid body and its surface temperature, respectively; T_{ch} is the average surface temperature of other solid bodies in the environment at temperature T_f, ε – relative radiation coefficient characteristic, for a given material, $\sigma = 5.67 \cdot 10^{-8}$ W/(m^2 K^4) – Stefan-Boltzmann constant.

The upper row of Eq. (1) represents convective heat transfer directly to the surroundings of the body, such as the surrounding air. The symbol h denotes the convection coefficient under these conditions. The lower row presents a heat balance that includes radiative heat transfer to other material bodies located at a considerable distance. Heat, treated as an extensive quantity, is expressed as the sum of the 'pure' convective heat flux, incorporating the convective component of Newton's coefficient, and the radiative heat flux directed toward distant material objects.

After introducing the assumption that, for good thermal conductors, the internal temperature of the body (θ) is equal to the surface temperature (T_h), Eq. (1) becomes nonlinear due to the presence of the temperature term raised to the fourth power. To linearize it, certain simplifications are applied: the ambient temperature and the temperature of the surrounding bodies are assumed to be similar ($T_h \approx T_f$). Under this condition, the radiation term can be expressed in the form of a convection-like equation, as shown in Eq. (2):

$$\varepsilon\sigma A_h\left(T_h{}^4 - T_{ch}{}^4\right) = h_r A_h\left(T_h - T_f\right), \tag{2}$$

or, after its prior linearization around, e.g., a certain average temperature $T_{av} = (T_h + T_f)/2$, where h_r is described by Eq. (3), [20]:

$$h_r \approx 4\varepsilon\sigma T_{av}{}^3. \tag{3}$$

As its result, the temperature term raised to the fourth power in Eq. (1) disappears. On the other hand, Newton's coefficient is expressed as the sum of the purely convective component h_k and the radiative component h_r.

Under steady-state conditions, the term involving enthalpy can be calculated as the heat generated by the heat-generating element, as in the case described in the work:

$$mc_p \frac{d\theta}{dt} = UI, \tag{4}$$

where: U, I are the voltage and current intensity, respectively, at the power input of the heat-generating element at a steady state.

In the rest of the article, the term h_k is used to emphasize the purely convective character of Newton's coefficient.

In the literature, two main models are known that calculate h_k in two extreme cases. The first concerns the situation when a solid body is surrounded by a medium and is in an open, unbounded space. In the second case, the medium is located in a gap between walls at a short distance from each other [21]. The first model describes phenomena in a typical open system. In the second case, the studied space is limited to a narrow, small gap, which may be located in another enclosed space [22]. As reported by the authors [23], both open and closed systems differ not only in their ability to interact with the environment, but also in the type and intensity of thermal phenomena occurring, which is reflected in the values of the coefficients in the equations describing these phenomena. The first model, mentioned earlier, describes the criterion for determining the value of h_k in unbounded space, under free convection conditions as in Eq. (5):

$$\mathrm{Nu} = \mathrm{B}\,(\mathrm{Gr}\cdot\mathrm{Pr})^{\mathrm{C}}, \tag{5}$$

where: Nu, Gr, Pr are the numbers of Nusselt, Grashof and Prandtl, respectively, and B, C are constant coefficients, the values of which are shown in Table 1 [22].

Table 1. B and C constants of the Eq. (5).

B	C	Gr·Pr
1	0	$\mathrm{Gr}\cdot\mathrm{Pr} < 10^{-3}$
1.18	0.13	$10^{-3} < \mathrm{Gr}\cdot\mathrm{Pr} < 500$
0.54	0.25	$500 < \mathrm{Gr}\cdot\mathrm{Pr} < 2\cdot10^{7}$
0.13	0.333	$2\cdot10^{7} < \mathrm{Gr}\cdot\mathrm{Pr} < 10^{13}$

In the case of the gap, rising convection currents from the warmer wall cannot develop freely and come into direct contact with descending currents from the cooler wall. As a result, fluid circulation is not fully developed. The way of heat flow is treated here as heat conduction between walls. The thermal conductivity coefficient, called equivalent λ_z is modified by applying a certain correction resulting from incomplete convection ε_k:

$$\lambda_z = \varepsilon_k\,\lambda, \tag{6}$$

where λ_z is the equivalent heat transfer coefficient, ε_k is the convection coefficient for this case, λ is the heat conduction coefficient for the fluid, for the arithmetic mean of the walls temperatures.

The correction ε_k is calculated from an experimental formula that relates the numbers Gr and Pr as in Eq. (7):

$$\varepsilon_k = \mathrm{D}\cdot(\mathrm{Gr}\cdot\mathrm{Pr})^{\mathrm{E}}, \tag{7}$$

where D and E are constants as in Table 2 [21].

Finally h_k is expressed by the formula:

$$h_k = \frac{\lambda_z}{\delta}, \tag{8}$$

where δ is the thickness of a gap.

Table 2. D and E constants of Eq. (7).

D	E	Gr·Pr
1	0	$\mathrm{Gr}\cdot\mathrm{Pr} < 10^{-3}$
0.105	0.3	$10^{3} < \mathrm{Gr}\cdot\mathrm{Pr} < 10^{6}$
0.4	0.2	$10^{6} < \mathrm{Gr}\cdot\mathrm{Pr} < 2\cdot10^{10}$

These two models for the two extreme cases of convection are described in detail. The authors expected that convection in the gap created between the heater (1) and the inner surface of the chamber (2) on the test rig sketched in Figs. 1 and 2 would not fully develop, and therefore the values of the convection coefficient h_k should be between those calculated in the literature models and the actual values obtained directly from the experiment. The topic was also very interesting due to the so-called scaling of convection cells, described in the introduction. It is not possible to clearly determine whether and how scaling may have occurred; however, the h_k values obtained using the ML model, being closer to reality, should allow for the rejection of some values derived from selected literature models.

3. The test rig

Figure 1 shows the sketch of the rig, along with its basic components.

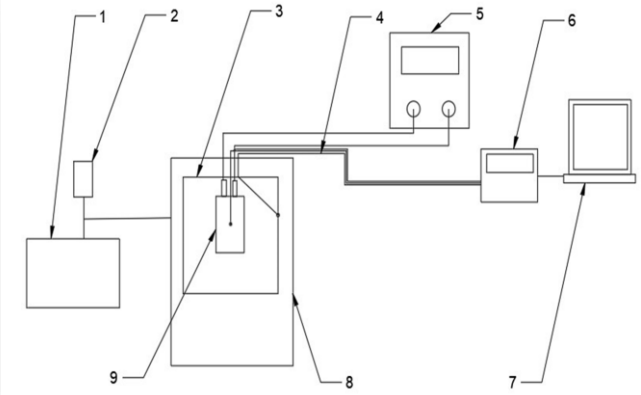

Fig. 1. The sketch of the rig: 1 − vacuum pump, 2 − digital vacuum gauge, 3 − chamber, 4 − thermocouple, 5 − DC power supply, 6 − Keithley multimeter, 7 − computer, 8 − desiccator, 9 – heater.

The experiments took place under dynamic vacuum at a pressure of about 300 Pa (2500 microns Hg). A cubic aluminium chamber along with a rectangular heater at its geometric centre, was placed in a desiccator that was connected to a vacuum pump. The chamber had an inner side that was 14 cm long. The heater had dimensions of 3 cm × 3 cm × 4 cm. The average resistance of the heater at 20°C was 9,6677621 Ω and the resistance of the cables connecting the heater at this temperature was 0,037 Ω.

Data from the rig were collected using the Keithley multimeter (hereafter referred to as the meter), which provided relatively accurate readings of the output signals in the form of resistance or voltage.

Figure 2 shows an axonometric mapping of the interior of the chamber, including the heater with external surface area A_h and temperature T_h (1), inner surface of the chamber with area A_{ch} and temperature T_{ch} (2). The gap, which is mentioned in the work topic, is created between the heater (1) and the inner surface of the chamber (2). In the gap, there is a fluid with temperature T_f. The black dots (3) mark the location of the thermocouples. Chamber (2) in Fig. 2 corresponds to position 3 in Fig. 1, which is located in the desiccator (8) in Fig. 1.

Thermocouples 1 and 3 are located at the intersection of the diagonals of the respective walls of the heater. Thermocouples 2 are located about 5 mm horizontally and 10 mm vertically from the edge of the heater wall. Thermocouples 4 and 5 located on the chamber wall are parallel to thermocouples 1 and 2. Thermocouple 6 is placed loosely in the space between the heater and the chamber wall and measures the temperature of the air in the chamber.

The temperature of the free ends of the K-type thermocouples was measured using a PT1000 sensor [24,25]. This was a class A sensor, so its tolerance is ± 0.15°C for the temperature range tested [26]. As for the thermocouples themselves [27], their tolerance in the range of tested temperatures was due to

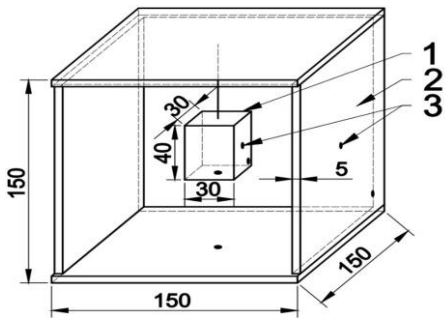

Fig. 2. Axonometric mapping of the interior of the chamber (2) including the heater (1) and temperature measurement locations (3). The gap is created between the heater (1) and the inner surface of the chamber (2) [18].

their initial calibration against each other. In addition, they were verified against PT100 [28]. They were assumed to have an accuracy of 0.2 K [29].

All temperature sensors were calibrated before the actual measurements.

The complete measurement cycle included reaching steady-state conditions at selected measurement points, including the stage after air evacuation, for a given heater power level. The test measurement time ranged between approximately 3−6 hours depending on the measurement series. However, this study focused exclusively on the phenomena occurring up to the activation of the vacuum pump, i.e. on phenomena involving only convection.

The quadratic approximation of the K-type thermocouple characteristic [30], in the form of Eq. (9), was used to convert the voltage signal in mV from the meter to degrees Celsius.

$$T = -0.1412 \cdot SEM^2 + 24.9231 \cdot SEM + 0.1462, \qquad (9)$$

where: T is the temperature value expressed in °C, SEM is the electromotive force value measured on the thermocouple in mV.

The detailed design of the experimental setup, along with more extensive descriptions, is presented in previously published works [18] and [19]. Each of these studies addresses distinct physical phenomena and targets different research objectives. Paper [18] focuses on the determination of the relative emissivity coefficient of black paint, essential for further analyses, under dynamic vacuum conditions at a pressure of 300 Pa. For the purposes of the present investigation, a value of 0.97 ± 0.03 for this coefficient (h_r) was adopted. Paper [19] discusses the use of an artificial neural network (ANN) to predict transient temperature responses and to assess the accuracy of steady-state (far-future) temperature distributions obtained during the heating process of a black-paint-coated heater, under power ranges corresponding to those employed in the current experiments. In contrast, the present study is devoted to the analysis of heat transfer in a gap under conditions of undeveloped convection.

3.1. The test results

As a result of temperature measurement at selected points of the test rig, a number of temperature characteristics changing over

time were obtained. An example plot of SEM in mV versus time is shown on Fig. 3.

Figure 3 consists of two parts. The first part, lasting up to approximately 4000 seconds (up to point P), presents the temperature evolution under convection conditions within the gap formed between the surfaces of the heater and the chamber, at all monitored points. The second part, after point P, shows the temperature changes under near-vacuum conditions, after the air has been evacuated, where heat transfer occurs via electromagnetic radiation. At this stage, the Newton coefficient decreases by the purely convective component, which impedes heat transfer in the region. The minimum amount of data for the so-called ANN Training Base (TB) is determined by the tangent method and is indicative – it contains data up to point A. The actual length of TB is longer and contains data up to point P.

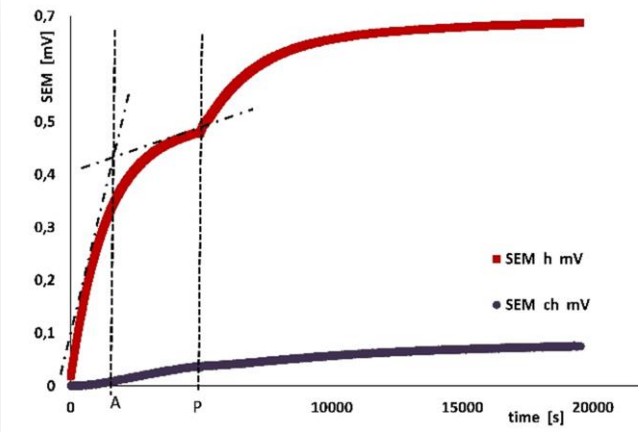

Fig. 3. Evolution of temperature over time as measured by thermocouples in mV on the heater – SEM h mV (top line), and on the inner surface of the chamber – SEM ch mV (bottom line). Point A on the OX-axis determines the minimum amount of training data for ANN returning the temperature value in steady states, point P – the actual amount of data constituting two so-called Training Bases.

3.2. Application of Artificial Neural Networks for the determination of selected steady-state temperature values

Figure 3 refers to the temperature evolution during the entire measurement cycle, as mentioned. The part that is the subject of this work covers the time from the beginning of the cycle to point P, where the vacuum pump was activated. The data up to the mentioned point P form TB for ANN, which included between 3.8 and 4.5 thousand data points recorded by the meter approximately every 3−6 seconds for all experiments. During the studies [19], it was determined that ANN was able to reproduce the curve $T = f(t)$ and predict the steady-state value of this function with relatively good accuracy, notably faster, approximately up to point A, determined for example using the tangent method (as shown in the figure). In this case, TB was significantly larger, which provides greater confidence that the values predicted by ANN relate to the sought steady-state temperature.

Figure 4 shows only the experimental data up to point P, which constitute TB. The temperature graphs are very predictable, with no distortions, so the chosen ANN may have had a very simple architecture.

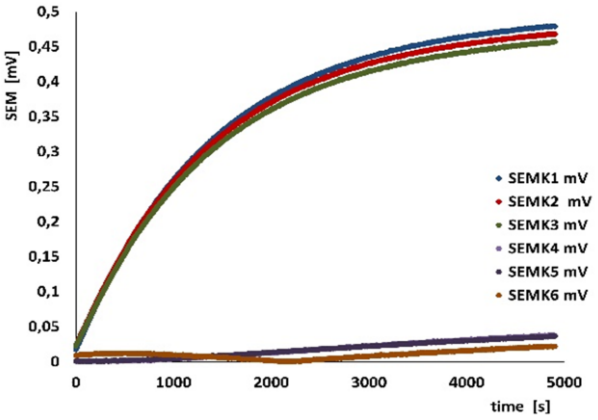

Fig. 4. Example training dataset for ANN. The data set at each monitored measurement point (1, 2, 3, 4, 5, 6) was free from significant noise and unexpected signal distortions, making a simple ANN architecture sufficient for effective learning, without the need for more advanced solutions such as Wavelet Neural Networks (WNN) or similar methods.

In this case, ANN was used to determine the steady-state temperature values [30], which − compared to the latest available experimental data at point P − differ by no more than 0.5–0.8 K across all convection-related experiments. The ANN used in this study [31] had a simple architecture: one neuron in the input layer (IN), several or a dozen neurons in the hidden layer (HL), and one neuron in the output layer (OUT). In general, the hidden layer may contain *m* neurons, and their number is typically selected by trial and error [32]. The network employed the backpropagation error algorithm [33]. Its principle is based on detecting an error, defined as the difference between the output signal from a given layer and the reference signal from the training sequence. This error is then corrected by adjusting the so-called weights, which are back propagated to all neurons providing input to the neuron where the error was detected.

A proprietary program based on the *nnet* package, integrated with the R programming language, was used in the study. The GNU R language belongs to the group of interpreted languages, and its source code is distributed under the GNU-GPL license [34]. This code is compatible with Excel spreadsheets.

Using ANN, the steady-state values of temperature expressed in mV (SEM) and the voltage at the terminals of the heat-generating element were ultimately determined. As demonstrated in [19], for simple functions − such as the temperature rise function during heating − using an ANN with a simple (IN-HL-OUT) structure allows for rapid prediction of the steady-state value with an accuracy of up to 0.03 K. The number of neurons (*m*) in the hidden layer should be at least $m = 6$ [33]. The length of the constructed TB is crucial for the learning process of the network and its sensitivity to disturbances in input data, which results from the nature of the backpropagation algorithm [35].

It is assumed that the steady state of the temperatures on the heater and the inner surface of the chamber is the state in which the temperature change rate at the designated points is less than 0.03 K/h. The number of neurons in the hidden layer was selected by trial and error, using statistical criteria.

3.2.1. Statistical functions for evaluating ANN data

One of the statistical techniques is regression analysis, which allows for determining the relationships between variables. In this case, the variables are the values returned by ANN for a specific subset of data, compared with their corresponding experimental data values. Pearson's coefficient is a tool that allows for the evaluation of whether there is a strong correlation between these quantities or not. A high correlation, i.e. a coefficient value close to 1, indicates that ANN accurately represents the real values. A low correlation, such as a value close to zero, suggests a poor fit of the model to the data. For this reason, Pearson's coefficient ($r_{y_{ei}y_i}$) in Eq. (10) and the commonly used root mean square error (RMSE) in Eq. (11) [36] were used to optimize the number of neurons in the hidden layer (HL)

$$r_{y_{ei}y_i} = \frac{\sum_{i=1}^{n}(y_{ei}-\overline{y_e})(y_i-\bar{y})}{\sqrt{\sum_{i=1}^{n}(y_{ei}-\overline{y_e})^2}\sqrt{\sum_{i=1}^{n}(y_i-\bar{y})^2}}, \quad (10)$$

$$RMSE(m) = \sqrt{\frac{\sum_{i=1}^{n}(y_{ei}-y_i)^2}{n}}, \quad (11)$$

where: y_{ei} – consecutive data from the experiment at the measurement point recorded in the i-th cell of the sheet, y_i is the corresponding value returned by ANN, $\overline{y_e}$ is the arithmetic mean value of experimental data, $\bar{y}$ is the arithmetic mean value of the results returned by ANN, n – the number of measurement data, m – the number of neurons.

As mentioned before, the selection of the best number of neurons was determined by the minimum value of RMSE and $r_{y_{ei}y_i}$ close to one. Tables 3 and 4 show an example comparison of the results obtained using ANN depending on the results of the selected functions.

Table 3. Example of optimization of the number of neurons m in HL based on the criteria of regression analysis for heater surface temperature.

m	$r_{y_{ei}y_i}$	RMSE	$T_{h\text{ANN}}$, °C
25	0.9999977	0.000345	38.37
28	0.9999977	0.000349	38.06
30	0.9999978	0.000343	38,02

Table 4. Example of optimization of the number of neurons m in HL based on the criteria of regression analysis for inner chamber surface temperature.

m	$r_{y_{ei}y_i}$	RMSE	$T_{ch\text{ANN}}$, °C
25	0.9378	0.00231	21.42
28	0.9986	0.00033	21.54
30	0.8287	0.00450	21.22

The columns devoted to the heater and the inner surface of the chamber contain, from the top, the number of neurons m in HL, RMSE and Pearson's coefficient values. In the last column, there is the temperature on a given surface in the far future, in steady states calculated by ANN with the mentioned number of neurons m in HL: $T_{h\text{ANN}}$ on the heater and $T_{ch\text{ANN}}$ on the inner surface of the chamber.

The best criterion fits were obtained for the heater: m = 28 and 30, and for the inner surface of the chamber: m = 28 and 25.

For ANN, the type of physical parameter whose value is to be determined is not important; only the quantity and quality of the data on which the network is trained matter. Figure 5 shows an example of graphs of temperature evolution in the form of the experimental dependence of SEM in mV on time and the response of ANN as it reaches its steady state, for the heater and for the inner surface of the chamber.

ANN was appropriately optimized by selecting the number of neurons m. Here, the selected number of neurons in the hidden layer (HL) was m = 28 (heater) and m = 25 (chamber). The thicker line represents the experimental data that constitute the training databases (TBs) for ANN, up to point P (Fig. 3).

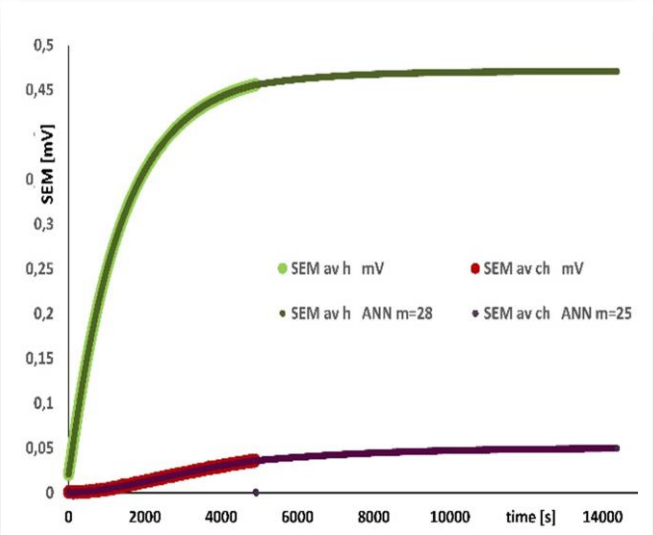

Fig. 5. Responses of ANN with an optimized number of neurons m, showing the evolution of temperature to its steady state value: for a higher heater temperature and a lower temperature on the inner surface of the chamber (thin lines in both mentioned cases). Training bases for ANN are indicated by bold lines.

As for the accuracy of the obtained RMSE and Pearson's coefficient values, they are shown with a large decimal expansion in Tables 3 and 4. The goal was to determine as accurately as possible which number of neurons in the hidden layer is most optimal.

Similarly, ANN was also used to determine the steady-state voltage at the heater terminals. Experimental data (thicker line) and ANN responses for m = 28 in HL are shown in Fig. 6. Compared to the latest available experimental data at point P, the values differ by no more than 6 mV across all convection-related experiments.

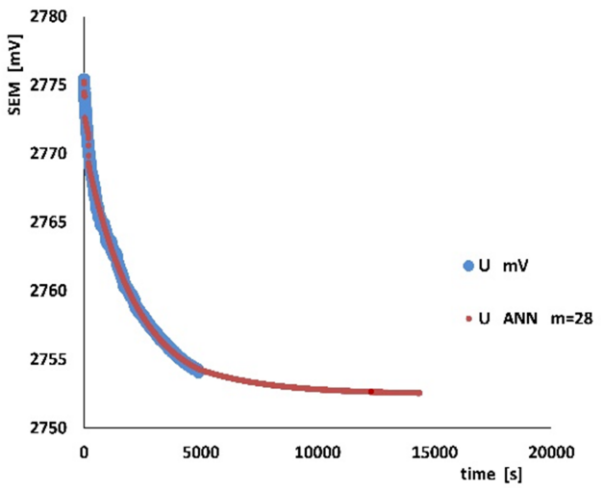

Fig. 6. Responses of ANN with an optimized number of neurons *m* determining the voltage on the heater in the steady state. Training bases for ANN are indicated by bold lines.

The computational power in further calculations was determined based on the steady-state voltage value returned by ANN and the average value of the heater resistance as in the formula in Eq. (12):

$$P = U^2/R, \tag{12}$$

where: P – the power of the heater, U – the value of the steady-state voltage returned by the ANN, R – the average resistance of the heater over the considered temperature range.

The heat flux dissipated by the heater has been reduced by the losses at the test rig as in Eq. (13):

$$\dot{Q} = P - \dot{Q}_\lambda - \dot{Q}_v, \tag{13}$$

where: $\dot{Q}$ is the heat flux dissipated by the heater in the chamber, $\dot{Q}_\lambda$ – heat flux losses conducted through the thermocouple wires connecting the heater to the meter, $\dot{Q}_v$ – enthalpy flux losses.

Thermal losses denoted as $\dot{Q}_\lambda$ are associated with the temperature gradient along the thermocouple wires and compensating leads, as well as with convection around the chamber in the desiccator environment $\dot{Q}_v$. These losses resulted from the routing of the measurement wires − from the test chamber, through the desiccator, and further to the measuring device located outside the desiccator.

In the experiment, six type K thermocouples were used, each with a diameter of 0.15 mm and a length of 1.2 m. The thermal conductivity coefficient was assumed to be λ = 20 W/(m K). Three of the thermocouples were used to measure temperatures of up to approximately 100°C, while the remaining three operated in the range of up to 30°C. Due to the unavailability of dedicated compensating cables (e.g. of type KX), 1.5 m long extensions were made using copper wires (λ = 400 W/(m K)) of the same diameter (0.15 mm), routed outside the desiccator. The temperature drop along the section outside the desiccator was estimated to be up to 10°C.

For twelve copper conductors (accounting for two leads per thermocouple), the estimated total thermal losses amounted to approximately $\dot{Q}_\lambda$ = 0.105 mW. In comparison, the heat power dissipated by the heater, calculated using Eq. (12), was approximately 5 W. For similar temperature conditions on the heater, chamber and outside the desiccator, the value determined using the method of total differential was characterized by an uncertainty of approximately 1.5 mW.

Therefore, it was concluded that the thermal losses $\dot{Q}_\lambda$ were negligible in this case.

Similarly, the temperature of the outer surface of the desiccator was comparable to the ambient temperature.

For this reason, both loss values: $\dot{Q}_\lambda$ and $\dot{Q}_v$ were neglected, and this way: $\dot{Q} = P$.

Nevertheless, considering future research and the potential need for higher measurement precision, these regions were identified as possible sources of uncertainty worth addressing in subsequent analyses.

Table 5 summarizes the steady-state temperatures returned by ANN with respect to the heat flux dissipated by the heater ($\dot{Q} = P$).

Table 5. Steady-state temperatures on the heater and on the inside surface of the chamber returned by ANN.

$\dot{Q}$, W	$T_{h\mathrm{ANN}}$, °C	$\Delta T_{h\mathrm{ANN}}$, K/h	$T_{ch\mathrm{ANN}}$, °C	$\Delta T_{ch\mathrm{ANN}}$, K/h	T_o °C
0.218	25.72	0.012	22.34	0.029	21.84
0.769	29.09	0.002	18.64	0.011	17.25
1.340	38.02	0.006	21.54	0.028	19.82
1.374	35.68	0.028	19.07	0.003	16.88
2.096	45.63	0.001	20.7	0.031	17.11
5.113	74.06	0.005	26.17	0.030	19.36

From left: $\dot{Q}$ – dissipated heat flux, $T_{h\mathrm{ANN}}$ – steady-state heater temperature returned by ANN and $\Delta T_{h\mathrm{ANN}} = f(\tau)$ being the rate of its increase over time τ, $T_{ch\mathrm{ANN}}$ – steady-state chamber surface temperature returned by ANN and $\Delta T_{ch\mathrm{ANN}} = f(\tau)$ being the rate of its increase over time, T_o – ambient temperature.

4. Linear method for determining the Newton's coefficient

The linear method (ML) for determining Newton's coefficient proposed in this work assumes its linear change with temperature, according to Eq. (14)

$$h_S = h_0 + \beta T, \tag{14}$$

where: h_S is the so-called "total" Newton's coefficient, containing both radiative and convective parts, determined by the ML method using the Solver function, h_0, β are constant, T is the temperature at the given location.

The only inconvenience in ML is the need to solve a system of several equations, where some solutions can only be approximate. For this purpose, the Solver function available in the Excel spreadsheet was used.

Solver is included by default in every office suite. It is integrated with Excel, which means that no external programs or coding are required. It works like a mini-math engine. Solver uses numerical methods such as Simplex LP, GRG Nonlinear,

or Evolutionary Solver. It handles nonlinear problems, constraints, and integers well. It helps solve various computational problems where no simple formula exists. It works by iteratively finding the best result for a selected cell, manipulating others until it meets the conditions.

Solver was used here to optimize the thermodynamics and heat transfer problem [37]. As shown in [38], the optimized Excel can successfully support optimization analyses of a similar type as in the article, but also in other areas of thermal technology, including recuperators.

The unknowns here are the temperatures prevailing in the space between the heater and the inner surface of the chamber T_{S1}, T_{S2}, and the constants h_0, β, which can be found from the system of equations with a unique solution:

$$\begin{cases} \dot{Q}_1 = A_h(h_0 + \beta T_{h1})(T_{h1} - T_{S1}) \\ \dot{Q}_1 = A_{ch}(h_0 + \beta T_{ch1})(T_{ch1} - T_{S1}) \\ \dot{Q}_2 = A_h(h_0 + \beta T_{h2})(T_{h2} - T_{S2}) \\ \dot{Q}_2 = A_{ch}(h_0 + \beta T_{ch2})(T_{ch2} - T_{S2}) \end{cases}, \quad (15)$$

where: $\dot{Q}_1$, $\dot{Q}_2$ are heat flux dissipation by the heater in the 1st or 2nd measurement, A_h and A_{ch} are the heater surface and the internal surface of the chamber, respectively, h_0 and β are constants from Eq. (14). T_{h1}, T_{h2} and T_{ch1}, T_{ch2} are experimental temperatures of the heater and the inner surface of the chamber in the 1st or 2nd measurement. T_{S1}, T_{S2} are the temperatures in the gap between the heater and the chamber returned by Solver, the average of which corresponds to the temperature of the heater surroundings.

To solve the system of Eq. (15), data from the two closest series of measurements with similar temperatures resulting from similar experimental powers were selected. The total surface areas for the heater and chamber are: A_h = 0.008996 m^2 and A_{ch} = 0.11745 m^2 [18]. The objective function used in Solver is the sum of squares, the unknowns being T_{S1}, T_{S2}, h_0, β. It is assumed that the value of β should be positive, but not zero, while h_0 can be zero. In this way, Newton's coefficient always increases with increasing power. Finally, from each case of power, two values of Newton's coefficient were calculated for the layer near the heater h_{hs} and for the layer near the inner surface of the chamber h_{chs}. The total value of coefficient h_s is the arithmetic average for a given series of measurements and the temperature in the gap T_S calculated by Solver is the arithmetic average of T_{S1}, T_{S2}. The results are shown in Table 6.

Table 6. Newton's heat transfer coefficient and gap temperature values calculated using the Solver function in ML.

$\dot{Q}$, W	T_S, °C	h_{hS}, W/(m²K)	h_{chS}, W/(m²K)	h_S, W/(m²K)
0.218	22.24	7.46	7.45	7.45
0.769	17.2	8.16	7.99	8.08
1.340	20.69	9.47	8.97	9.22
1.374	18.22	10.02	9.48	9.75
2.096	19.85	11.72	11.30	11.51
5.113	25.33	12.83	12.82	12.82

4.1. Comparison of experimental results for different theoretical models

Based on the known relative emissivity of the black paint ε, the radiative component of the heat transfer coefficient h_r was calculated using Eq. (2).

Subsequently, the total heat transfer coefficient h was determined from experimental data using Eq. (1). By subtracting the radiative component h_r, from the total value of h, the convective part of the Newton heat transfer coefficient h_{ke} was directly determined from the experiment.

Using Eq. (5), the convective part of Newton's coefficient calculated in the open model h_{ktoc} was calculated.

The gap thickness is assumed to be the distance between the heater surface and the inner surface of the chamber, which is 5.5 cm. Using Eqs. (6)–(8), the convective part of Newton's coefficient in the gap model h_{ktgc} was calculated.

On the other hand, the convective part of Newton's coefficient h_{kS} in the proposed ML method was calculated according to Eq. (15), as the difference between the Newton's coefficient determined using the Solver function in Eq. (14) h_S and the radiative component h_r (Eq. (2))

$$h_{kS} = h_S - h_r, \quad (16)$$

where: h_{kS} and h_S are the convective part of Newton's coefficient and its total value in ML, respectively.

Table 7 presents the values of the convective parts of Newton's coefficient for selected theoretical models and compares them with the values obtained in ML and the experimental values, accurate to the second decimal place. From left: convective part of Newton's coefficient obtained experimentally h_{ke}, convective part of Newton's coefficient obtained in ML h_{kS}, convective part of Newton's coefficient calculated in the gap model h_{ktgc}, convective part of Newton's coefficient calculated in the open model h_{ktoc}.

Table 7. Comparison of the convective parts of Newton's coefficient under limited convection conditions from the experiment with its values from different models.

$\dot{Q}$, W	h_{ke}, W/(m²K)	h_{kS}, W/(m²K)	h_{ktgc}, W/(m²K)	h_{ktoc}, W/(m²K)
0.218	1.33	1.75	1.33	4.34
0.769	1.78	2.39	1.85	5.77
1.340	2.72	3.32	2.11	6.41
1.374	2.99	3.71	2.12	6.42
2.096	3.58	5.26	2.37	7.05
5.113	4.28	5.46	2.81	8.14

In Fig. 7, it can be seen that the values of the convective part of Newton's coefficient obtained experimentally h_{ke} and calculated from ML h_{kS} lie between their counterparts from the open and gap model.

Figure 7 illustrates that the analysed relationship is generally satisfied, with the exception of the first and second positions from the origin of the coordinate system, which correspond to the lowest tested power levels: 0.218 W and 0.769 W. In these

specific cases, the experimental values of the Newton heat transfer coefficient (h_{ke}) closely match those obtained using the gap model (h_{ktgc}) whereas the values predicted by ML are consistently higher than the actual measured values.

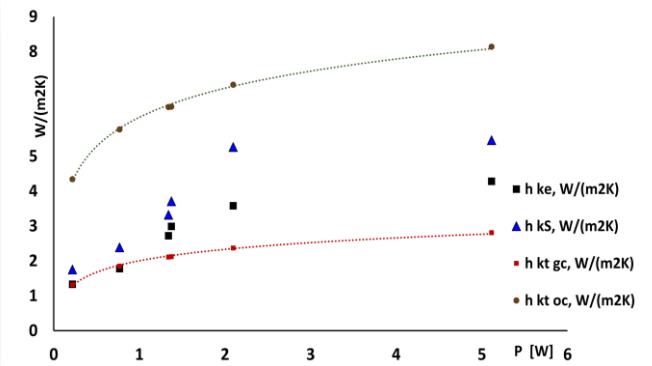

Fig. 7. Validation of the ML model based on comparison of the convective part of Newton's coefficient h_{ke} as a function of (here) heater power P. Experimental data are compared with values obtained from the ML model (h_{kS}), the gap model (h_{ktgc}), and the open model (h_{ktoc}). Slightly higher ML predictions confirm the presence of convection suppression in the gap.

For all other cases − particularly those involving higher power levels − a clear convergence is observed between the experimental data and the values predicted by the ML model. Notably, the ML-based estimations tend to approach the arithmetic mean of the results derived from the two classical models commonly cited in the literature.

In general, slightly higher ML predictions confirm the presence of convection suppression in the gap.

Nevertheless, the ML approach appears to offer a relatively simple yet more accurate means of estimating the Newton heat transfer coefficient across the tested power range of the heater.

5. Overview of materials, methods and measurement uncertainties

In terms of the applied methods, the study was divided into an experimental part and a computational part, utilizing numerical software, including an ANN and the Solver module. The work is a continuation of previous research concerning the determination of the relative emissivity coefficient of black paint. The value of this coefficient is one of the key parameters used to determine the convection coefficient in the gap.

The research method described and applied in "Emissivity measurement of black paint using the calorimetric method" [18] was the calorimetric method, which requires maintaining the system, both internally and externally, in stable conditions for a relatively long period to obtain appropriate parameters in steady-state conditions, i.e. states in the distant future. Such procedures are generally time-consuming and expensive, which is a drawback of this method. On the other hand, all values of material constants are typically determined under steady-state conditions due to their stability and the precisely defined physical conditions under which they are determined. Papers [18] and [19] describe and illustrate in detail the construction of the experimental setup. Figure 2 of this paper presents an axonometric mapping of the chamber's interior, including the heater's location and temperature measurement points, taken directly from [18], along with the main dimensions of the chamber placed in the desiccator (8), in accordance with the sketch of the test rig (Fig. 1).

Since the time required to reach a steady state in convection conditions should be significantly shorter due to the faster stabilization of temperature, and one research cycle included both the temperature evolution at selected locations under convection conditions and in a vacuum (after air evacuation from the chamber), there was uncertainty whether the system actually reached the required steady state in its first stage, i.e. under convection conditions, necessary for determining steady-state convection coefficients. The criterion for achieving a steady state was a temperature change of less than 0.03 K per hour.

To verify whether the experimentally measured temperatures at selected points corresponded to their steady-state values, an ANN was used. The network architecture included: 1 neuron in the input layer, m neurons in the hidden layer (selected by trial and error), and 1 neuron in the output layer, as described in "Numerical prediction of steady-state temperature based on transient measurements" [19]. Due to its simplicity, this architecture is commonly used to predict values in the so-called distant future (steady states).

Here, two data analysis methods were used: ANN and the least squares approximation method, to predict steady-state temperature values based on short-term measurements. It was found that in the case of heater heating functions in the chamber, ANN was able to predict steady-state temperature values after only about one-third of the experiment time required by the classical calorimetric method. Thus, the use of ANN effectively reduced the duration of the experiments.

The ANN program was written in R, version 3.4.2 (X86 = 64-in 64-mgw32/x64), using the nnet library, which contains the Fit Neural Network module. Due to ANN's compatibility with Excel, the Solver module was also used to solve systems of equations with four unknowns, characterized by its ease of use and wide availability.

The values of the Newton coefficient h_{kS} calculated in ML were then compared with values obtained using two literature models mentioned in this work and derived from experiment h_{ke}. These models describe: natural convection in an open system, allowing full development of convection in an unbounded space, and in a gap-type system, suppressing its mechanisms.

The value of the relative emissivity coefficient of black paint, along with the error of the method, is presented in [18]. The obtained values ranged from 0.958 ±0.07 to 1.049 ±0.102. Assuming that the relative emissivity coefficient should not exceed 1, values greater than 1 were excluded from further calculations. The overestimation of the coefficient resulted from the very low power of the heater, which led to relatively large measurement errors. The average value of the coefficient, after rejecting the overestimated values, was 0.97 ±0.03, and this value was used for further calculations. Determining its value was a necessary step in calculating the radiative part of h_r (Eq. (2)).

The length of the elements needed to determine surface areas was measured using a precise micrometer, with a reading error of 0.01 mm and a systematic error of 0.001 mm. A measurement

error of ±0.000011 m was adopted. The ambient temperature was measured using a PT100 sensor, with an accuracy of ±0.2 K.

Type A thermocouples, calibrated against each other and verified against the PT100 sensor, also had an accuracy of ±0.2 K.

Voltage was measured using a Keithley Model 2000 multimeter, capable of measuring DC voltage up to 100 mV, AC voltage up to 10 V, and resistance up to 100 Ω. In the range of up to 100 mV, the basic accuracy was 0.0035% + 0.0002, which did not significantly affect thermocouple temperature measurements, as the additional error in the 0–100°C range was below 15.3 mK (0.015 K).

The heater supply voltage, required for calculating the design power, was measured with an accuracy of ±1 mV (0.001 V).

The resistance of the heater at ambient temperature was measured up to 100 Ω and was 9.667621 Ω. After accounting for the resistance of the measurement leads, the total resistance was 9.70472 ±0.00084 Ω. The heat stream from Eq. (12) was calculated with an uncertainty of about 1 mW.

For illustrative purposes, additionally, the heater power was also estimated based on power supply readings, with an accuracy of 0.1 W.

The absolute uncertainty in determining h_r using the total differential method (based on Eq. (2)) consists of the corresponding partial uncertainties associated with the respective differentials, as shown below:

$$\begin{cases} \frac{\partial h_r}{\partial T_h} = \frac{\varepsilon\sigma(4{T_h}^3)}{T_h - T_f} - \frac{\varepsilon\sigma({T_h}^4 - {T_{ch}}^4)}{(T_h - T_f)^2} \\ \frac{\partial h_r}{\partial T_{ch}} = -\frac{\varepsilon\sigma(4{T_{ch}}^3)}{T_h - T_f} \\ \frac{\partial h_r}{\partial T_f} = -\frac{\varepsilon\sigma({T_h}^4 - {T_{ch}}^4)}{(T_h - T_f)^2} \end{cases} . \tag{17}$$

Since all temperatures were measured with an accuracy of ±0.2 K, and after calculating and summing all partial uncertainties, the total uncertainty of the determined h_r within the examined range is approximately 0.3 W/(m²·K) on average.

Similarly, the partial derivatives for calculating the uncertainty h are calculated based on a modified Eq. (1), due to the steady state on the heater, Eq. (18):

$$\begin{cases} \frac{\partial h}{\partial \mathrm{P}} = \frac{1}{A_h(T_h - T_f)} \\ \frac{\partial \mathrm{h}}{\partial A_h} = -\frac{P}{{A_h}^2(T_h - T_f)} \\ \frac{\partial h}{\partial T_h} = \frac{P}{A_h(T_h - T_f)^2} \\ \frac{\partial h}{\partial T_f} = -\frac{P}{A_h(T_h - T_f)^2} \end{cases} , \tag{18}$$

The average uncertainty of h in the examined range is approximately 0.2 W/(m²·K), with the highest value about 0.4 W/(m²·K) occurring at the lowest heat flux dissipated by the heater. The average uncertainty of the difference $h - h_r$, treated as the square root of the sum of squares of the individual components, is 0.36 W/(m²·K).

In the context of using ANN and Solver, the classical understanding of measurement accuracy − referring to instrument limitations, tolerances or random conditions − becomes less relevant. Instead, the concept of prediction accuracy or numerical solution accuracy becomes crucial. In the case of ANN, the model quality was assessed using the root mean square error (RMSE) and the Pearson correlation coefficient, whose values are presented in Tables 2 and 3. For Solver, it was expected that the final result would fall between values determined according to the models describing natural convection in an open system and in a gap system.

6. Reconstructing the rig with a view to further research

In this article, the simple formula of ML in the form of Eq. (14) is analysed for the "total" Newton coefficient.

Now a formula is proposed as in Eq. (19) for its convective part only (h_k):

$$h_k = h_0 + \beta T, \tag{19}$$

Research should be continued in two directions:

1. Analysis of the damping effect of the gap geometry (i.e. reduction of its thickness and/or height),
2. Investigation of the influence of temperature difference on convection enhancement.

In reality, both mechanisms interact and partially cancel each other, so the experimental rig should be reconstructed to quantitatively and qualitatively determine their interplay.

6.1. Idealized model "Nusselt sphere"

In the first conceptual approach, it is proposed to use the idea of the "Nusselt sphere," where the gap of thickness L is formed between two concentric spheres with radii, respectively: R_h − radius of the heater (inner sphere), with external surface area $A_h = 4\pi {R_h}^2$, R_{ch} − radius of the chamber (outer sphere), with internal surface area $A_{ch} = 4\pi {R_{ch}}^2$:

$$R_{ch} - R_h = L. \tag{20}$$

Temperature sensors are installed: in the heater ($T_h = T_h(R_h)$ − heater surface temperature), in the surrounding air (with T_o), on the chamber wall ($T_{ch} = T_{ch}(R_{ch})$).

6.1.1. Heat conduction in the heater

The Poisson equation with a uniform volumetric heat source in a steady state can be written as:

$$\frac{1}{r^2}\frac{d}{dr}\left(r^2 \lambda_g \frac{dT_h}{dr}\right) + q_v = 0 \ , \ r \in [0, R_h], \tag{21}$$

where: $q_v = \dot{Q}/(4/3 \cdot \pi {R_h}^3)$ is the volumetric heat generation rate (so-called "internal heat sources").

Boundary conditions**:**

- at the heater centre (symmetry):

$$\left.\frac{dT_h}{dr}\right|_{r=o} = 0, \tag{22}$$

- at the heater surface:

$$-\lambda_g \frac{dT_h}{dr}\Big|_{r=R_h} = \alpha(T_h - T_o) + \varepsilon\sigma\left({T_h}^4 - {T_o}^4\right). \quad (23)$$

6.1.2. Heat balance in the gap

The heat flux dissipated by the heater leaving it (Eq. (13)) passes through the air in the gap and reaches the chamber wall:

$$\dot{Q} = A_h h_{kh}(T_h - T_o) + A_h \varepsilon\sigma\left({T_h}^4 - {T_o}^4\right) = A_{ch} h_{kch}(T_o - T_{ch}), \quad (24)$$

*w*here: h_{kh} – convective heat transfer coefficient at the heater surface, h_{kch} – convective heat transfer coefficient at the chamber surface.

6.1.3. Extended formula for h_k

To account for both the position and temperature dependence, it is proposed:

$$h_k(r,T) = h_0 + \gamma\frac{r}{L} + \beta T(r)\ ,\ r \in [R_h, R_{ch}]. \quad (25)$$

The corresponding steady-state energy balance for $r \in [R_h, R_{ch}]$ can be written as:

$$\dot{Q} - A_h \varepsilon\sigma\left({T_h}^4 - {T_{ch}}^4\right) = \left(h_0 + \gamma\frac{r}{L} + \beta T(r)\right)\times A_h(T_h - T_o). \quad (26)$$

Measurements at $r = R_h$, $r = L/2$, $r = R_{ch}$ allow the determination of h_0, γ, β.

If technical challenges arise, a simplified model can be adopted by omitting the position-dependent term:

$$h_k(r) = h_0 + \beta T(r), \qquad r \in [R_h, R_{ch}]. \quad (27)$$

This linear model underlies ML described in the article.

6.1.4. Modified ANN on the reconstructed rig

In the future, the use of more advanced artificial neural networks (ANN) will be advisable. Valuable insights in this area are provided in articles [39−41]. In [39] two methods for modelling the ground-coupled heat pump system (GCHP) were compared: artificial neural networks (ANN) and adaptive neuro-fuzzy inference systems (ANFIS). The article used the coefficient of determination (R^2) to assess the model fit. This coefficient is calculated using the formula:

$$R^2 = 1 - \frac{\sum_{i=1}^{n}(y_{ei} - \overline{y_e})}{\sum_{i=1}^{n}(y_{ei} - y_i)}, \quad (28)$$

where: y_{ei} – consecutive data from the experiment at the measurement point recorded in the *i*-th cell of the sheet, y_i is the corresponding value returned by the ANN, $\overline{y_e}$ is the arithmetic mean value of experimental data, n – the number of measurement data.

Equation (28) is used to evaluate how well the model explains the variability of the observed data, with a focus on the quality of fit. Due to its simple structure and ease of application to specific cases, it may serve as an additional statistical criterion in future analyses.

It is also advisable to facilitate the ANN learning process. For example: similar to [40], to appropriately process the input data based on the weights assigned to them – both manually and using statistical functions such as RMSE (root mean square error) or R^2. This approach supports the ANN learning process, improving prediction accuracy by eliminating noise and random disturbances from measurement devices during the data pre-processing stage.

In the case of highly sensitive measurement equipment, it may be observed that during variations in the size of the gap, the temperature − which influences the function $h_k(r)$ − evolves in an unexpected manner. It is therefore essential to determine whether such fluctuations are due to measurement noise or constitute a significant aspect of the underlying physical phenomenon occurring within the gap.

Wavelet functions, as discussed in [41], may prove particularly useful in such analyses. In the referenced study, the authors compare traditional artificial neural networks (ANNs) with wavelet neural networks (WNNs) for modelling a solar air heater system.

In WNNs, wavelet basis functions − such as those derived from mother wavelets like Haar or Symlets − are employed in the hidden layers instead of conventional activation functions such as tanh or sigmoid.

Networks trained in this manner exhibit high flexibility when analysing nonlinear and non-stationary signals. Wavelet transformations decompose a signal across multiple scales (frequencies) and locations (time), allowing the network to capture both fine-grained features and potential disturbances originating from the measurement apparatus.

6.1.5. Influence of atmospheric composition

An additional advantage of the improved rig is the possibility of testing various gas mixtures in the gap, as the desiccator, which is an element of the setup, allows for testing different gases, effectively separating the atmosphere in the gap from the external environment. It is possible to study, for example, nanofluids, mixtures of air with water vapour, and air with CO_2. Considering radiation and absorption by gases is essential:

- monoatomic and diatomic gases (except CO and HCl) are nearly transparent to thermal radiation,
- triatomic gases (CO_2, H_2O) significantly absorb and emit in specific frequency bands.

For example:

- at approximately −50°C, both water vapour (H_2O) and carbon dioxide (CO_2) absorb heat,
- around 0°C, CO_2 becomes inactive, while H_2O strongly absorbs heat with the wavelength near $\lambda \approx 6$ μm,
- at 25°C, H_2O dominates in radiation and absorption,
- at 100°C, water vapour still intensively absorbs heat, while CO_2 remains nearly inactive.

Studying the influence of these effects on the heat balance in the gap and on the coefficients $h_k(r)$, $h_{kh} = h_k(R_h)$, $h_{kch} = h_k(R_{ch})$ (e.g. by comparison with pure nitrogen) seems to be a valuable

direction for future research, especially in times when there is so much talk about the topic of the so-called "climate warming".

7. Conclusions

This study presents a simplified ML method for determining the Newton coefficient under conditions of limited (undeveloped) convection in a gap, within the heater power range of approximately 0.2 W to 5 W. A weak linear dependence of the Newton coefficient on temperature was assumed.

To verify the value of the Newton coefficient obtained using ML, the first stage involved experimental determination of its convective component h_{ke} and experimental radiative component h_r. The convective part calculated by ML h_{kS} was obtained by subtracting the radiative component h_r from the "total" Newton coefficient determined using the Solver program h_S, and was subsequently compared with the convective part measured experimentally h_{ke}. The radiative component was determined based on previous experimental studies, taking into account measurements of the relative emissivity of the black paint covering the heater and the internal surfaces of the chamber.

It was demonstrated that the experimental values of the convective part of the Newton coefficient fall between the values obtained from the gap model h_{ktgc} (lower bound Fig. 7) and those calculated using ML. Moreover, both the experimental and ML-derived values fall between the results obtained from literature based models (gap model h_{ktgc} and open model gap model h_{ktoc} – lower and upper bounds at Fig. 7, respectively). And the values obtained using ML slightly exceed those real ones, derived from the experiment.

- It was thus shown that convection in the gap of the test rig is suppressed due to geometric constraints, meaning the convective flow could not fully develop.
- This validates the ML-based approach.
- ML seems to be a very simple method for estimating the convective heat transfer coefficient in a gap under limited convection conditions.

Artificial Neural Networks (ANN) were employed in this study to determine selected steady-state parameters, namely, the temperature and the voltage at the heater terminals. The number of neurons *m* in the hidden layer (HL) was selected using a trial-and-error method, optimizing RMSE and Pearson's correlation coefficient as objective functions. Additionally, a separate optimization problem was solved to find the solution to a system of four equations using the Solver program used in ML.

In light of the obtained results, a reconstruction of the test rig is planned to enable further investigation of convection phenomena in the gap and to validate ML methods over a broader range of measurement conditions.

References

[1] McAdams, W.H. (1954). *Heat Transmission*. McGraw-Hill Book Company.

[2] Lienhard IV, J.H., & Lienhard V, J.H. (2019). *Heat Transfer Textbook*. Phlogiston Press Cambridge.

[3] Aubin, D. (2008). The memory of life itself: Bénard's cells and the cinematography of self-organization. *Studies in History and Philosophy of Science, Part A*, 39(3), 359−369. doi: 10.1016/j.shpsa.2008.06.007

[4] Aliouane, I., Kaid, N., Ameur, H., & Laidoud, H. (2021). Investigation of the flow and thermal fields in square enclosures: Rayleigh-Bénard's instabilities of nanofluids. *Thermal Science and Engineering*, 25. doi: 10.1016/j.tsep.2021.100959

[5] Mathews, J., & Hymavathi, T. (2024). Unsteady magnetohydrodynamic free convection and heat transfer flow of Al2O3–Cu/water nanofluid over a non-linear stretching sheet in a porous medium. *Archives of Thermodynamics*, 45(1), 165–173. doi: 10.24425/ather.2024.150449

[6] Mathews, J., & Hymavathi, T.(2024). Unsteady flow of silica nanofluid over a stretching cylinder with effects of different shapes of nanoparticles and Joule heating. *Archives of Thermodynamics*, 45(3), 115–126.445. doi: 10.24425/ather.2024.151222

[7] Houdek, G., & Dupret, M.A.(2015) Interaction Between Convection and Pulsati. *Living Reviews in Solar Physics*, 12(8), doi: 10.1007/lrsp-2015-8, 10.48550/arXiv.1601.03913

[8] Husain, S., Adil, M., Arqam, M., & Shabani, B. (2021). A review on the thermal performance of natural convection in vertical annulus and its applications. *Renewable and Sustainable Energy Reviews*, 150, doi: 10.1016/j.rser.2021.111463

[9] Misale, M., Fossa, M., & Tanda, G.(2014). Investigation of free convection in a vertical water channel. *Experimental Thermal and Fluid Science*, 59, 252−257. doi: 10.1016/j.expthermflusci.2014.01.022

[10] Pretot, S., Zeghmati, B., & Palec Le, G. (2000), Theoretical and experimental study of natural convection on a horizontal plate. Applied Thermal Engineering, 20(10), 873−891. doi. 10.1016/S1359-4311(99)00067-8

[11] Radziemska, E., & Lewandowski, W.M, (2001). Heat transfer by natural convection from an isothermal downward-facing round plate in unlimited space, Applied Energy, 68(4), 347−366. doi: 10.1016/S0306-2619(00)00061-1

[12] Rohsenow, W.M., & Hartnett, J.P. (1998). *Handbook of heat transfer*. The McGraw-Hill Companies.

[13] Ghoben, Z.K., & Hussein, A.K. (2002). Natural Convection Inside a 3D Regular Shape Enclosures - A Brief Review. *International Journal of Heat and Technology*, 40(1), 32−246. doi: 10.18280/ijht.400128

[14] Chithrakumar, V., Venugopal, G., & Rajkumar, M. (2019). Convection in vertical annular gap formed by stationary heated inner cylinder and rotating unheated outer cylinder. *Heat and Mass Transfer*, 55, 2873–2888. doi: 10.1007/s00231-019-02614-0

[15] Petrichenko, M., & Petrochenko, M. (2022). Hydraulics of natural convection flows in building walling with air gap. *Magazine of Civil Engineering*, 26, 63−69. doi: 10.5862/MCE.26.8

[16] Said, S.A.M, & Krane, R.J. (1990). An analytical and experimental investigation of Natural Convection Heat Transfer in vertical channels with single obstruction. *International Journal of Heat Mass Transfer*, 33, 1121−1134. doi: 10.1016/0017-9310(90)90245-P

[17] De Giorgi, L., Bertola, V., & Cafaro, E.(2011). Thermal convection in double glazed windows with structured gap. *Energy and Buildings*, 43(8), 2034-2038. doi:10.1016/j.enbuild.2011.03.043

[18] Pelińska-Olko, E. (2023). Emissivity measurement of black paint using the calorimetric method. *Archives of Thermodynamics*, 44(3). doi:10.1007/s10765-011-1010-2

[19] Lewkowicz, M., & Pelińska-Olko, E. (2018). Numerical prediction of steady state temperature based on transient measurements. *MATEC Web of Conferences*, 240(05024). doi: 10.1051/matecconf/201824005024

[20] Hobler, T. (1971). *Heat movement and exchangers*. WNT Warszawa (in Polish).

[21] Pudlik, W. (2012). *Heat exchange and exchangers.* Wydawnictwo Politechniki Gdańskiej (in Polish).
[22] Kostowski, E. (2003). *Collective work*. Wydawnictwo Politechniki Śląskiej (in Polish).
[23] Mikielewicz, J., & Mikielewicz, D. (2024). Influence of thermodynamics on the development of technology and science. *Archives of Thermodynamics*, 45(2), 51–61. doi: 10.24425/ather.2024.150851
[24] Batagelj, V., & Bojkovski, R.J. (2011). Calibration by comparison of platinum resistance thermometers using slow resistance bridges. *Journal of Thermophysics*, 32, 1409−1417. doi: 10.1007/s10765-011-1010-2
[25] Wędrychowicz, W. (2015). *Temperature measurement with metal and semiconductor resistance thermocouples*. Wydawnictwo Politechniki Wrocławskiej (in Polich).
[26] Lundström, H., & Mattsson, M. (2020). Radiation influence on indoor air temperature sensors: Experimental evaluation of measurement errors and improvement methods. *Experimental Thermal and Fluid Science*, 115. doi: 10.1016/j.expthermflusci.2020.110082
[27] Wędrychowicz, W. (2017). *Temperature measurement with thermocouples.* Wydawnictwo Politechniki Wrocławskiej (in Polish).
[28] Liu, H.T., Shao, D., & Li, B.Q. (2012). Theory Analysis of Thermocouple Temperature Measurement. *Applied Mechanics and Materials*, 239−240, 749−753. doi: 10.4028/www.scentific.nett/AMM.239-240.749
[29] Liu, B., Huang, Q.H., & Wang, P.Y. (2020). Influence of sur rounding gas temperature on thermocouple measurement. *Case Studies in Thermal Engineering*, 19. doi: 10.1016/j.csite.2020.100627
[30] Czujniki termoelektryczne. Katalog-Edycja 2023. Termoaparatura, Wrocław (in Polish). https://termoaparatura.com.pl/media/wysiwyg/docs/type-k-table-pl.pdf [accessed 22 Feb. 2025].
[31] Tadeusiewicz, R., & Szaleniec, M. (2015). *Neural Network Lexicon*. Wydawnictwo Fundacji „Projekt Nauka" (in Polish).
[32] Cantú-Paz, E. (2003). Pruning neural networks with distribution estimation algorithms. *Genetic and Evolutionary Computation Conference* (GECCO, LNCS, 2723, 790–800), 12−16 Jul., Chicago, IL, USA. doi: 10.1007/3-540-45105-6_93
[33] Pavlidis, N.G., Tasoulis, O.K., Plagianakos, V.P., Nikiforidis, G., & Vrahatis, M.N. (2005). Spiking Neural Network training Using Evolutionary Algorithms. In: *Proceedings. 2005 IEEE International Joint Conference on Neural Networks*, vol. 4, 2190–2194. doi: 10.1109/IJCNN.2005.1556240
[34] Ripley, B., &. Venables, W. (2022). Package 'nnet'. https://cran.r-project.org/web/packages/nnet/nnet.pdf [accessed 22 Feb. 2025].
[35] Rigler, A.K., Irvine, J.M., & Vogl, T.P. (1991). Rescaling of variables in back propagation learning. *Neural Networks*, 4, 225−229. doi: 10.1016/0893-6080(91)90006-Q
[36] StatSoft Electronic Statistics Textbook (1984−2024). https://www.statsoft.pl/textbook [accessed 22 Feb. 2025].
[37] Stachurski, A. (1999). *Optimization Basics.* Oficyna Wydawnicza Politechniki Warszawskiej (in Polish).
[38] El-Awad, M.M., & Al-Saidi, M.S. (2022). Excel as an educational platform for design analyses of fluid-thermal systems. *World Journal of Engineering and Technology*, 10(20), 434−443. doi: 10.4236/wjet.2022.102025
[39] Esen, H., Inalli, M., Sengur, A., & Esen, M. (2008). Artificial Neural Networks and adaptive neuro-fuzzy assessments for ground-coupled heat pump system, *Energy and Buildings*, doi: 10.1016/j.enbuild.2007.10.002
[40] Esen, H., Inalli, M., Sengur, A., & Esen, M (2008). Forecasting of a ground-coupled heat pump performance using neural networks with statistical data weighting pre-processing, International Journal of Thermal Sciences, 47(4), 431−441. doi: 10.1016/j.ijthermalsci.2007.03.004
[41] Esen, H., Ozgen, F., Esen, M., & Sengur, A. (2009). Artificial neural network and wavelet neural network approaches for modelling of a solar air heater. *Expert Systems with Applications*, 36(8), 11240−11248. doi: 10.1016/j.eswa.2009.02.073